

# Enhanced Hydro-Actuation and Capacitance of Electrochemically Inner-Bundle-Activated Carbon Nanotube Yarns

Wonkyeong Son,<sup>◆</sup> Jae Myeong Lee,<sup>◆</sup> Sungwoo Chun, Seongjun Yu, Jun Ho Noh, Hyeon Woo Kim, Sung Beom Cho, Seon Jeong Kim,\* and Changsoon Choi\*



Cite This: *ACS Appl. Mater. Interfaces* 2023, 15, 13484–13494



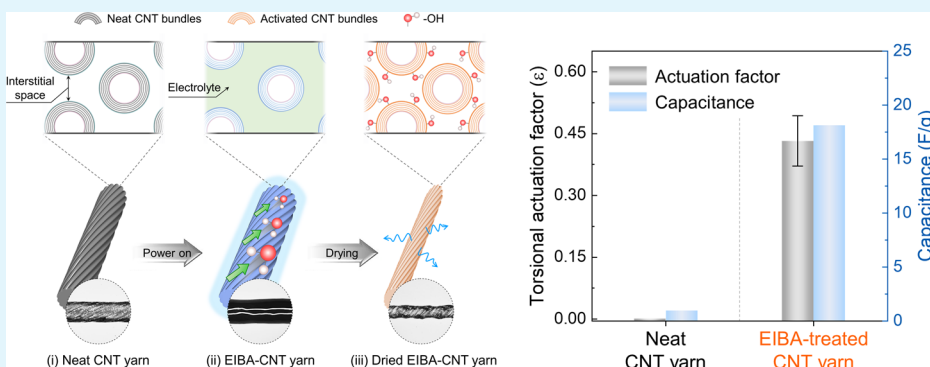
Read Online

ACCESS |

Metrics & More

Article Recommendations

Supporting Information



**ABSTRACT:** Recently, several attempts have been made to activate or functionalize macroscopic carbon nanotube (CNT) yarns to enhance their innate abilities. However, a more homogeneous and holistic activation approach that reflects the individual nanotubes constituting the yarns is crucial. Herein, a facile strategy is reported to maximize the intrinsic properties of CNTs assembled in yarns through an electrochemical inner-bundle activation (EIBA) process. The as-prepared neat CNT yarns are two-end tethered and subjected to an electrochemical voltage (vs Ag/AgCl) in aqueous electrolyte systems. Massive electrolyte infiltration during the EIBA causes swelling of the CNT interlayers owing to the tethering and subsequent yarn shrinkage after drying, suggesting activation of the entire yarn. The EIBA-treated CNT yarns functionalized with oxygen-containing groups exhibit enhanced wettability without significant loss of their physical properties. The EIBA effect of the CNTs is experimentally demonstrated by hydration-driven torsional actuation (~986 revolutions/m) and a drastic capacitance improvement (approximately 25-fold).

**KEYWORDS:** electrochemical activation, inner bundles, carbon nanotube yarns, hydro-actuations, capacitances

## INTRODUCTION

Carbon nanotube (CNT) yarns fabricated by twisting the forest-drawn nanobundles<sup>1</sup> exhibit great potential in diverse fields because of their unique structures. On the macroscale, well-aligned CNTs absorb the severe stress applied during yarn spinning and form a single helix braid;<sup>1,2</sup> their distorted chiral scrolls store the mechanical energy. On the microscale, millions of nanobundles and mesoporous interbundle gaps present inside the yarns provide a dense and enormous electrochemical effective surface area.<sup>3</sup> This nanobundle-braided structure implies that CNT yarns can be promising candidates for yarn-based actuators and electrochemical energy storage devices. However, their nonresponsiveness to polar media and the limited capacitance induced from the intrinsic inertness of the graphitic structure remain critical obstacles that hinder the practical uses of these yarns.<sup>4</sup> To overcome these limitations, it is essential to activate the CNT yarns both holistically and homogeneously using carbon functionalization methods.

Oxygen plasma treatment, a type of carbon oxidation strategy, has been widely used to activate CNTs in laboratories and industries owing to its convenience, short application time, and possibility of scaling up.<sup>5,6</sup> During the treatment, plasma composed of high-energetic oxygen ions and highly reactive radicals generate defective sites on the nanotube wall, leading to chemical reconstruction of the nanotube with oxygen-containing functional groups.<sup>5–7</sup> As a result, the surface polarity of the CNTs change; the functional groups in the CNTs affect their surface energy as well as increase their hydrophilicity and chemical reactivity.<sup>8</sup> Indeed, various applications of CNT activation by plasma treatment have

Received: November 17, 2022

Accepted: February 21, 2023

Published: March 1, 2023



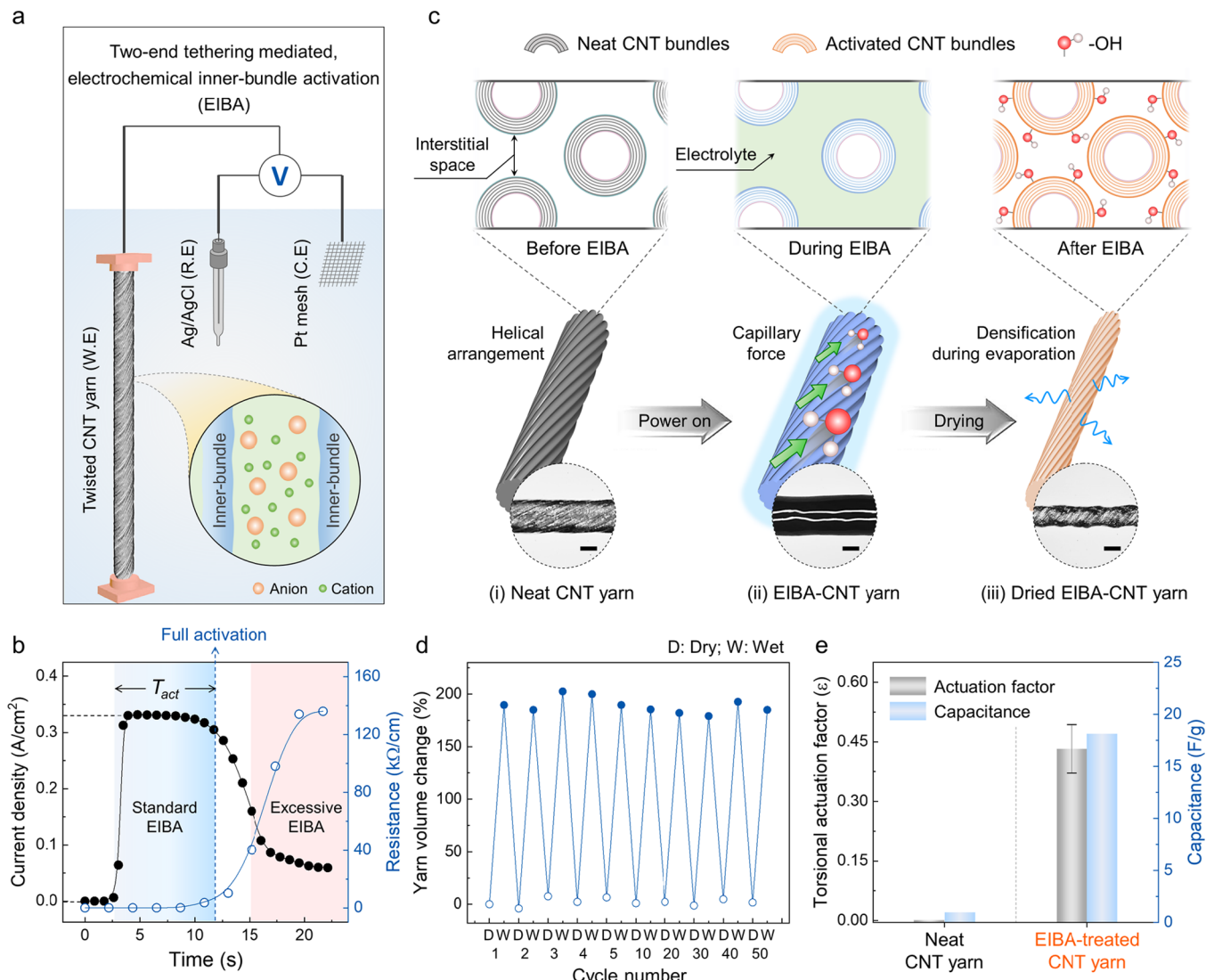


**Figure 1.** EIBA of macroscopic CNT yarns resulting in a large volume expansion via a massive electrolyte infiltration. (a) Schematic of the EIBA treatment setup, which consisted of twisted CNT yarns (the working electrode), Ag/AgCl (the reference electrode), a Pt mesh (the counter electrode), and 0.1 M Na<sub>2</sub>SO<sub>4</sub> (the liquid electrolyte). Inset: schematic showing the infiltration of the anions and cations of the electrolyte between the adjacent CNTs within the yarns. (b) Time dependence of the current density and yarn resistance under a constant electrochemical voltage of 4.5 V (vs Ag/AgCl). (c) Schematics and cross-sectional views of the twisted CNT yarn (containing microbundles) after the sequential EIBA process and drying, showing internal activation with hydroxyl group formation, and optical images of the (i) neat CNT yarn with a helical arrangement, (ii) EIBA-CNT yarn with capillary force,<sup>30</sup> and (iii) dried EIBA-CNT yarn with evaporation-induced densification (scale bar: 100  $\mu$ m). (d) Reversible volume change (in percent) in the dried EIBA-CNT yarns in response to water over 50 cycles. (e) Comparison of the torsional actuation factor and specific capacitance of a neat CNT yarn with those of the corresponding dried EIBA-CNT yarns.

been reported until recently. Ham et al. fabricated plasma-treated multiwalled CNT (MWNT)-based gas, humidity, and immuno-sensors;<sup>6</sup> He et al. fabricated a water-responsive actuator and implantable supercapacitors with plasma-treated CNT yarns.<sup>9,10</sup> Shao et al. and Adusei et al. reported yarn-based supercapacitors with increased electrochemical capacitances using oxygen plasma treatment.<sup>11,12</sup> However, despite several advantages, plasma treatment has an inherent limitation for CNT activation. The effects of plasma are limited to the superficial CNT layers, leaving the inner region unfunctionalized.<sup>7,13,14</sup> Although CNTs in the outer layer are functionalized by a direct reaction with the highly energetic species, the shadowing of outermost CNT layers and the short penetration depth of plasma does not allow the active species to penetrate inside.<sup>15</sup> Moreover, the extremely short lifetimes of the species

(less than 1 ms) also hinder them to reach the internal area.<sup>15,16</sup> Consequently, in most cases, oxygen plasma penetrates only up to a few micrometers from the surface. Thus, the development of holistically and homogeneously activated CNTs by plasma treatments has rarely been reported to date.<sup>14,15</sup> Although plasma treatment is obviously an excellent CNT activation method, it is undesirable for one-dimensional and nano-bundle-braided CNT yarns, which have limited microscale sizes, surface areas, and volumes. In other oxidizing methods, such as acid treatments or air oxidation (including thermal, photonic, and gas treatment) using a fluid-type oxidant, the reactants can infiltrate the interbundle gaps.<sup>17–20</sup> However, the harsh experimental conditions (e.g., strong acids or high temperatures) required for these methods tend to degrade the mechanical and electrical properties of

CNTs.<sup>21</sup> Thus, a novel activation approach is required for the effective activation of nano-bundle-braided CNT yarns.

Electrochemical oxidizing treatment performed in an aqueous electrolyte solution can be an interesting alternative.<sup>3,22–28</sup> While a bias potential or current is applied to the CNT yarn immersed in the electrolyte, the electrostatic forces and capillary effects arising from the mesoporous bundle gaps offer an effective electrolyte infiltration and a uniform charge injection deep inside the fiber.<sup>28</sup> Foroughi et al. showed that a potentiostat voltage applied to CNT yarns can increase the volume via electrochemical double-layer charge injection.<sup>2</sup> Then, the ions reaching the inner areas of the nanobundles constituting the yarn caused an enormous electrochemical reaction on the whole active surface area, resulting in a homogeneous and holistic construction of oxygen-containing groups on the CNT yarn. These reported observations suggest that electrochemical oxidation is the most suitable method that can effectively activate the surface of the CNT yarns as well as the individual nanobundles inside the yarn. These effects cannot be realized by using conventional oxidizing methods.

Herein, we propose a new type of CNT yarn with enhanced hydro-actuation and innate capacitance achieved by applying the electrochemical inner-bundle activation (EIBA) process to two-end-tethered CNT yarns. When the bias voltage was applied, the tethers at both ends of the yarn suppressed the mechanical actuation-induced losses, which were driven by the electrolyte infiltration, and thus, maximized the morphological changes (e.g., a remarkable increase in the yarn diameter and volume). Benefiting from the swelled yarn volume, the EIBA-CNT yarn actuator provided a large torsional stroke of 986 revolutions/m and a fast peak rotary speed of 933 rpm. In contrast, the neat CNT yarn generated only a negligible torsional stroke. Additionally, the assembled yarn supercapacitor showed a noticeably enhanced areal capacitance of 72.8 mF/cm<sup>2</sup>, which was 25-fold higher than that shown by the neat CNT yarn supercapacitor. We expect that these inner-bundle-activated CNT yarns to be a cornerstone for constructing advanced yarn-based applications discussed here.

## RESULTS AND DISCUSSION

### EIBA-CNT Yarns with Electrolyte Infiltration-Induced Yarn Volume Expansion

**Yarn Volume Expansion.** Figure 1a illustrates the experimental setup for the EIBA process. The setup had a three-electrode system consisting of the twisted CNT yarns as the working electrode, an Ag/AgCl reference electrode, and a Pt mesh counter electrode immersed in a 0.1 M Na<sub>2</sub>SO<sub>4</sub> aqueous electrolyte. The EIBA process was conducted by applying a potentiostat voltage to the two-end tethered working electrode (twisted CNT yarns). When a bias voltage was applied, the tethers at both ends of the yarn allowed an immediate electrolyte infiltration but inhibited any mechanical actuation induced by the volume expansion. As a result, the nano-gaps in the aligned CNTs within the yarn underwent drastic expansion with the increased internal pressure (inset of Figure 1a and Movie S1, Supporting Information).

Meanwhile, the voltage application time is an important parameter that determines the degree of activation. The activation time ( $T_{act}$ ) is defined as the time required to reach 90% of the maximum value in the current density plot during the constant voltage application. Figure 1b shows that  $T_{act}$  was 10 s at a given applied voltage (4.5 V vs Ag/AgCl); this provides information on the termination of the EIBA process for full activation. Furthermore, we observed a drop in the

current density beyond the standard EIBA region because of severe activation. The yarn resistance drastically increased from 0.043 to 136 kΩ/cm in this excessive EIBA region due to the destruction of the π–π conjugation structure. Unless stated otherwise, the CNT yarns were processed up to the standard EIBA region at a constant applied voltage of 4.5 V (vs Ag/AgCl). Although the voltage amplitude can be further increased, the resulting activation time reduced to the order of milliseconds (e.g., 400 ms at 10 V) may be unfavorable for specific control of the degree of activation (Figure S1, Supporting Information). Figure S2 shows the dependence of the maximum current, activation time, input power, and consequent total electrical energy on the applied voltage. When the applied voltage was increased from 3.0 to 4.5 V (vs Ag/AgCl), the activation time decreased from 30 to 10 s, indicating that these two parameters are inversely related. It should be noted that the total input energy required for the EIBA process converged to approximately 1.8 J per treatment, irrespective of the applied voltage in a given range. This low-energy consumption feature can be advantageous over conventional plasma treatments in terms of energy efficiency. The activation conditions, such as the input power and applied time, for the EIBA-CNT yarns are compared with those of the previously reported plasma-treated CNT fibers or yarns in Figure S3. Based on the total input energy, our input power and applied time (0.18 W and 10 s, respectively) were significantly lower than those observed in the previous studies.

Twist-spun yarns were prepared by continuously spinning a bunch of CNTs derived from a vertically grown forest. The as-prepared CNT yarns exhibited a single helix structure with highly aligned CNT bundles, revealing a constant bias angle (Figure 1c-(i)). Despite the tight twist, the neat CNT yarns still contained interstitial spaces among the CNTs owing to weak van der Waals forces.<sup>29,30</sup> With the progress of the electrochemical charge injection during the EIBA, the massive electrolyte infiltration into the yarn assisted by capillary forces<sup>31</sup> induced swelling of the CNT interlayers, resulting in an increase in the yarn volume (Figure 1c-(ii)). Interestingly, dried EIBA-CNT yarns exhibited completely different morphological changes, including yarn shrinkage, which is attributed to the surface tension-based densification that occurs during water evaporation (Figure 1c-(iii)). Specifically, the average outer diameter of the CNT yarn measured from the scanning electron microscopy (SEM) images (Figure S4a,b) decreased from approximately 0.224 to 0.158 mm, corresponding to the increase in the average yarn density from 0.42 to 0.85 g/cm<sup>3</sup>. Additionally, the magnified SEM images revealed surface micro-buckling (Figure S4c,d) and condensation of the CNT bundles (Figure S4e,f). These tightly connected CNTs produce an enhanced capillary force for fast solvent absorption.<sup>32</sup> The EIBA-CNT yarns exhibited large reversible volume changes upon hydration and dehydration for 50 consecutive cycles (Figure 1d). This unprecedented large volume expansion (~200%) driven by water absorption cannot be simply interpreted as a result of the CNT activation alone. Generally, the dense and tightly bundled structure of the yarn produced via extensive twists is unfavorable for electrochemical voltage-induced ion diffusion inside the twisted yarns.<sup>33</sup> Therefore, the CNT bundle near the yarn center does not participate in the volume expansion resulting from electrolyte infiltration as effectively as the bundles near the surface do.<sup>34</sup> Additionally, these electrochemical volume changes are directly translated into torsional and tensile actuations to relieve the

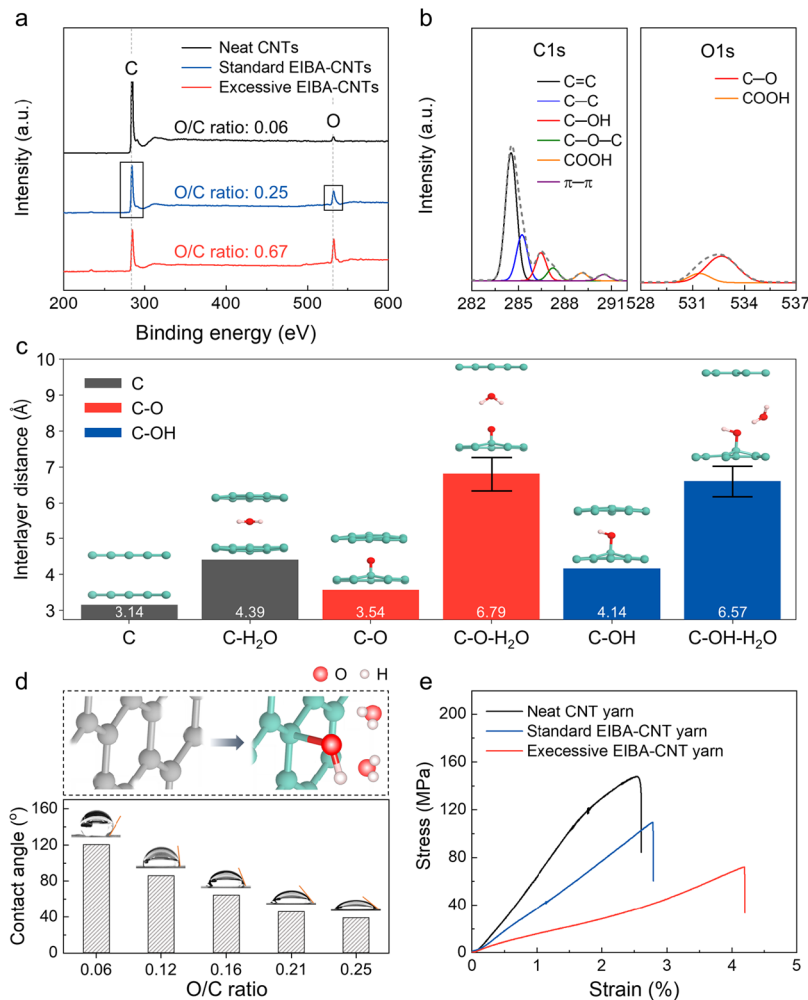


**Figure 2.** Chemical and mechanical characterizations of the CNT yarns. (a) XPS profiles of the neat CNT and standard EIBA-CNT (4.5 V vs Ag/AgCl for 10 s) yarns along with those of the excessive EIBA-CNT (4.5 V vs Ag/AgCl for 20 s) yarns. (b) High-resolution C 1s (left) and O 1s (right) XPS spectra of the standard EIBA-CNT yarns marked in (a). (c) DFT-calculated interlayer distance of the bilayer graphene before and after water adsorption. (d) Measured contact angles (CAs) between a water droplet and the CNT sheets with increasing O/C ratios during the EIBA process. Top illustrations show atomic structures of a neat CNT (left) and hydroxyl-group-functionalized EIBA-CNT surface (right). (e) Stress-strain curves of the neat CNT, standard EIBA-CNT, and excessive EIBA-CNT yarns.

induced internal pressure without destroying the one-chiral McKibben structure of the yarn. However, the present CNT yarn was prepared in a two-end tethered state and was subjected to charge injection for electrochemical activation without any type of unwanted actuation. Hence, the increased internal pressure was only consumed to extend the interstitial space between the CNTs, which facilitated successive ion diffusion from the surface to the center of the yarn. That is, CNT inner-bundle activation was achieved.

The result of Figure 1e exhibits that the proposed EIBA process drastically improved the intrinsic performance of the neat CNT yarn in terms of torsional actuation and capacitance. Based on the following fact that the twisted yarn can represent untwisting actuation when the yarn volume is expanded,<sup>2,35–37</sup> the torsional actuation factors ( $\varepsilon$ ) of the neat and EIBA-treated CNT yarns upon water absorption were calculated and compared by using the equation:  $\varepsilon = R \times 1/T$ , where  $R$  and  $T$  are the number of revolutions and inserted twists, respectively. Although the calculated actuation factor of the neat CNT yarn was close to zero due to innate hydrophobicity stemming from the inert graphitic bonding,<sup>38</sup> the value increased significantly up to 0.43 after the EIBA processing

of the yarn. Furthermore, the EIBA-treated CNT showed a 25-fold increased specific capacitance compared with that of the neat CNT yarn. Notably, this value is much higher than that of the previously reported plasma-treated CNTs (2–6 times).<sup>12,39,40</sup> From the aforementioned results, we postulate that in our case, the electrochemical activation occurred throughout the inner-bundle structure of the macroscopic CNT yarns.

**Chemical and Mechanical Characterizations.** The degree of activation of the CNT yarns was easily tuned by varying the applied time (up to 30 s) or voltage (3.0–4.5 V vs Ag/AgCl). The changes in the chemical composition of the CNT yarn before and after the EIBA process were investigated by X-ray photoelectron spectroscopy (XPS) and Raman spectroscopy. As shown in Figure 2a, the XPS spectra revealed distinct carbon and oxygen peaks at 284 and 532 eV, respectively. Meanwhile, increasing the degree of activation reduced the carbon peak intensity progressively and increased the oxygen peak intensity (Figure S5a–d). As a result, the calculated oxygen/carbon (O/C) atomic ratios increased from 0.06 to 0.25 regardless of the applied voltage or time in a given range, representing the high degree of oxygen functionalization

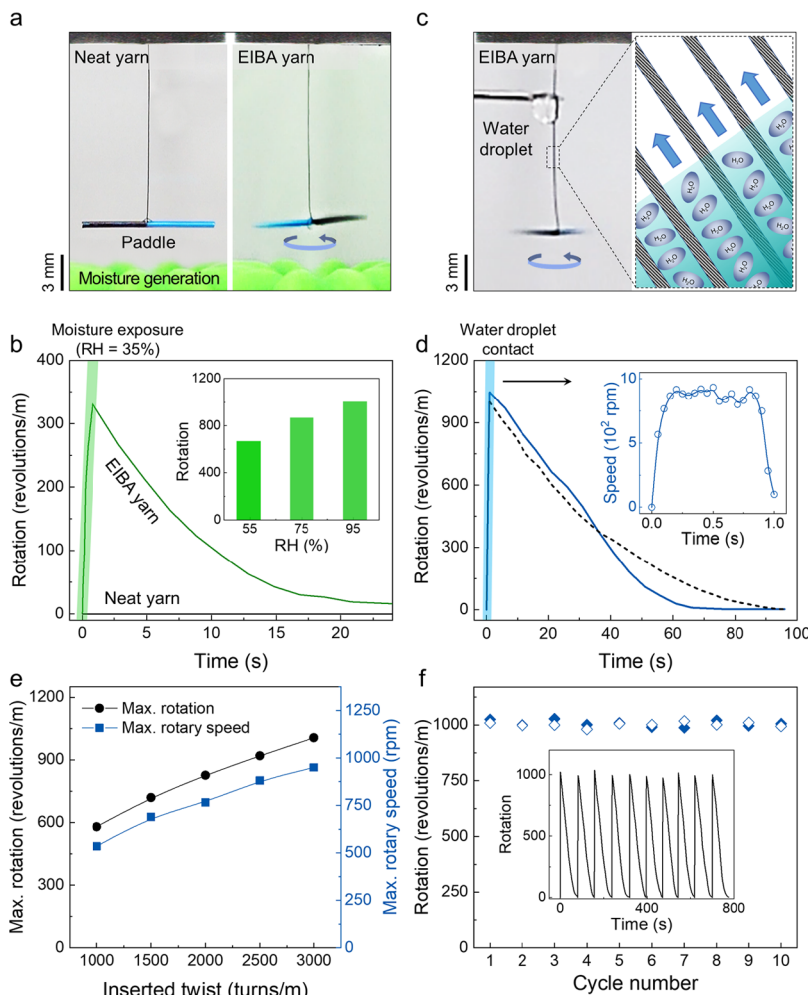


**Figure 3.** Moisture- and water-driven mechanical actuation of the EIBA-CNT yarns. (a) Photographs of the neat CNT (left) and EIBA-CNT yarns (right) captured after exposing them to moisture generated from a humidifier (green patch at the bottom of the photograph). Weight of the paddle attached at the bottom end of yarn was 10 mg. Left image: the hanging paddle does not show any movement; Right image: a rotary actuation is generated when exposed to moisture. (b) Torsional strokes versus time for the neat and EIBA yarns upon moisture exposure ( $\text{RH} = 35\%$ , green region) and moisture removal. Inset: rotation of the EIBA-CNT yarn under various other humidity conditions. (c) Photograph of the EIBA-CNT yarns with a paddle (10 mg) when in contact with a water droplet and an enlarged view showing water diffusion along the nano-gaps (arrows) between the aligned CNTs. (d) Comparison of time-dependent torsional stroke for EIBA-CNT yarns under water (solid line) and moisture ( $\text{RH} = 95\%$ , dashed line) stimulation. Inset: time-dependent rotary speed within the blue region (d). (e) Dependence of maximum torsional stroke and rotary speed on the amount of inserted twist. (f) Number of forward (open symbol) and reverse (close symbol) rotations during the actuation cycles, driven by water absorption and desorption. Inset shows the time dependence of the rotation numbers for 10 consecutive cycles for a torsional EIBA yarn with a twist density of 3000 turns/m.

of the CNTs (Figure S5e). The functional groups were also confirmed by the Raman spectroscopic analysis. The intensity ratio ( $I_{\text{D}}/I_{\text{G}}$ ) of the two peaks at 1590 and 1350/cm, corresponding to the G and D bands, is summarized in Figure S6. The  $I_{\text{D}}/I_{\text{G}}$  ratio, indicating the extent of defect density in the graphitic carbon structure, increased from 0.51 to 0.81 after the standard EIBA process, which supports the above XPS results. Excessive activation after applying 4.5 V (vs Ag/AgCl) for longer than  $T_{\text{act}}$  introduced a higher oxygen content, as shown by the O/C ratio of 0.67 and the  $I_{\text{D}}/I_{\text{G}}$  ratio of 1.05. Figure 2b shows the high-resolution C 1s and O 1s spectra of the standard EIBA-CNT yarns. The detailed functional group types and amounts were analyzed by deconvoluting the C 1s and O 1s peaks using Gaussian peak fitting (Figure S7), referring to the following bonds in the C 1s spectra: C=C (284.4 eV), C–C (284.8 eV), C–OH (286.4 eV), C–O–C (287.7 eV), and COOH (288.8 eV) (Table S1). Peaks

corresponding to the C–O (532.7 eV) and COOH (531.5 eV) bonds were also identified in the O 1s spectra. Notably, the content of the hydroxyl group (C–OH) is much higher than that of the epoxy (C–O–C) or carboxyl (COOH) groups in both the standard and excess EIBA-CNTs. Therefore, it is speculated that the formation of C–OH through electrochemical treatment is crucial for activating the CNT yarns, including their water-driven volume increase (Figure 1d). Using density functional theory (DFT) calculations, the water-driven volume expansion of the CNTs can be mimicked by comparing the interlayer distance of the bilayer graphene with and without water molecules. Figure 2c shows the influence of various oxygen functional groups on the DFT-calculated distance of the CNT interlayers during water absorption. For the neat CNTs, the water-driven expansion length was 1.25 Å, including the flat shape of the adsorbed water molecule. In contrast, with the functionalization of epoxy and hydroxyl, the

water-driven expansion of the CNT interlayers became active with lengths of 3.25 and 2.43 Å, respectively. In addition, the adsorbed water molecules showed nonflat shapes, which promote further expansion of the CNT interlayers. This implies that the interaction between the oxygen functional groups and the water molecules plays a critical role in the expansion of the region between the CNT interlayers and their actuating behavior. Additionally, the local polarization of the oxygen-functionalized CNTs enables strong interactions with the polar water molecules,<sup>41</sup> and consequently, substantially higher interactivity and wettability of the CNTs are expected. The electrochemical wetting effect of the CNT yarns was experimentally confirmed by measuring the contact angle (CA) of a water droplet. Figure 2d shows the dependence of the water contact angle on the degree of CNT oxidation. The neat CNT sheets (with an O/C ratio of 0.06) displayed their hydrophobic nature with a CA of approximately 120°. The EIBA process proportionally reduced the CA between the water droplet and the sheet surface up to 38° with the increment in the O/C ratio (~0.25), i.e., the EIBA-treated CNTs became more hydrophilic with enhanced wettability. Extrinsic hydrophilicity may be attributed to the introduction of hydroxyl (C–OH) groups onto the CNT surface during the treatment (top insets in Figure 2d). The mechanical properties of the neat and EIBA-CNT yarns were also characterized and compared using stress–strain curves (Figure 2 e). The mechanical strength and modulus of the neat CNT yarn were 147.9 and 58.5 MPa, respectively. The EIBA process lowered the strength and modulus values by 25.6% (109.5 MPa) and 37.9% (39.4 MPa), respectively, while the elongation strain before fracture was increased by 9.02% ( $\epsilon = 2.78\%$ ). Moreover, excessive activation further reduced the mechanical strength (72.1 MPa) and modulus (17.2 MPa). However, the fracture elongation of the excessive EIBA-CNT yarn progressively improved up to 4.2% possibly due to the newly formed hydrogen bonds between the oxygen-containing functional groups as well as the micro-buckling at the yarn surface after the activation process.<sup>42,43</sup> Noteworthy is that despite the reduced toughness (69.4%) of the standard EIBA-CNT yarns, they were still strong enough to be able to withstand the high internal pressure caused by water absorption and the resulting volume expansion (Figure 1d), enabling reversible and large torsional actuation (Figure 3b,d).

**Hydration-Driven Torsional Actuation of the EIBA-CNT Yarns.** Because of such excellent mechanical properties and large hydro-volume changes, the yarns with a one-chirality McKibben structure<sup>44</sup> can exhibit an untwisting behavior based on the fact that the actuation performances of yarn actuators are significantly affected by their volumetric changes.<sup>2</sup> We further investigated the hydration-driven torsional actuations of the EIBA-CNT yarns as a proof of the CNT bundle activation with high water interactivity and compared them with those of the neat CNT yarn. Figure 3a shows that 15-mm-long and 160-μm-thick EIBA-CNT yarns were supported at one end with a heavy paddle attached to the other end. The generated torsional hydro-actuation was recorded using a high-speed camera and then interpreted by frame-to-frame analysis. When the EIBA-CNT yarn was stimulated by moist air, the fast water-molecule infiltration resulted in a large untwisting (330 revolutions/m), while the neat CNT yarn did not show any movement under the same condition (Figure 3b). This rotation performance was gradually improved with an increase in relative humidity (RH) and finally reached 966 revolutions

per meter at an RH of 95%. The excellent moisture-triggered torsional actuation of the EIBA-CNT yarns enabled the fabrication of a high-performance electric generator that could convert the rotational energy into electric energy (Figure S8). A 4-cm-long EIBA-CNT yarn was fabricated to hold several magnetic circles at one end; these circles were located at the center of triple-solenoid copper coils (Figure S8a). When the EIBA-CNT yarn was exposed to moisture (RH = 95%), electricity (peak voltage of 12 mV) was induced in the copper coils due to the reversible forward and reverse rotations of the magnet (Figure S8b).

Benefiting from such a sensitive response against water molecules, our EIBA-CNT yarns also produced an excellent rotation in response to water droplets (left image in Figure 3c). Especially, the nanochannels between the condensed CNT bundles enabled rapid water diffusion along the helical direction with yarn volume expansion (right image in Figure 3c). As shown in Figure 3d, when the entire body (length of 15 mm) of EIBA-CNT yarn was in contact with a water droplet, a torsional stroke of ~14.8 rotations (986 revolutions/m) (solid line) was observed for a hydration time of ~1 s. This observed torsional stroke was similar to that (966 revolutions/m) obtained under a 95% RH (dashed line). The corresponding maximum rotary speed was 933 rpm (97.7 rad/s) (inset of Figure 3d). Importantly, the water-saturated EIBA-CNT yarn returned to its original state after dehydrating completely because the inter-nanotube connections can act as returning springs (Figure S4f). However, the returning process (approximately 75 s) occurred noticeably slower than the untwisting actuation (approximately 1 s), which may be attributed to the strong interactions between the functional groups and the water molecules (e.g., hydrogen bonding).<sup>45</sup>

The ability to actuate a twisted yarn depends on the inserted twist if the change in the length of the yarn during the torsional actuation is negligible.<sup>2</sup> According to the equation,  $\alpha = \tan^{-1}(2\pi rT)$  (where  $r$  represents the radius of the yarn,  $\alpha$  denotes the bias angle of the yarn, and  $T$  represents the amount of inserted twist per initial yarn length), the inserted twist density is proportional to the bias angle of the CNT fibrils with respect to the yarn direction.<sup>36</sup> Figure S9 shows that the bias angles determined from the SEM images of the EIBA-CNT yarns having different twist densities are approximately consistent with those calculated using the above equation. The slight difference between the measured and calculated results can be ascribed to the reduction in the bias angle after the EIBA process (Figure S4f). The maximal torsional stroke and corresponding peak rotary speed increased quasi-linearly with increasing (inserted) twists (Figures 3e and S10). Unless otherwise specified, the hydro-actuation results were obtained from an EIBA-CNT yarn with a twist density of 3000 turns per meter. The generated torque per yarn mass was 402 mN·m/kg, which was calculated by considering the moment of inertia ( $8.33 \times 10^{-11} \text{ kg}\cdot\text{m}^2$ ) of the paddle weighing 10 mg (a hundred times heavier than that of the yarn) and the average rotor acceleration (580 rad/s<sup>2</sup>). This specific initial torque generated in the EIBA-CNT yarns is comparable to that reportedly observed in the case of hygromorphing torsional actuators.<sup>37,46</sup> However, the maximal rotation (986 revolutions per meter) was still lower than those of the reported fiber- or yarn-based actuators with water-absorbing guest materials such as graphene oxide (GO) hydrogel,<sup>47</sup> poly(3,4-ethylenedioxythiophene)–poly(styrenesulfonate) (PEDOT:PSS),<sup>36</sup> and chitosan (CS)<sup>48</sup> (Table S2). Figure 3f and its inset show a reversible

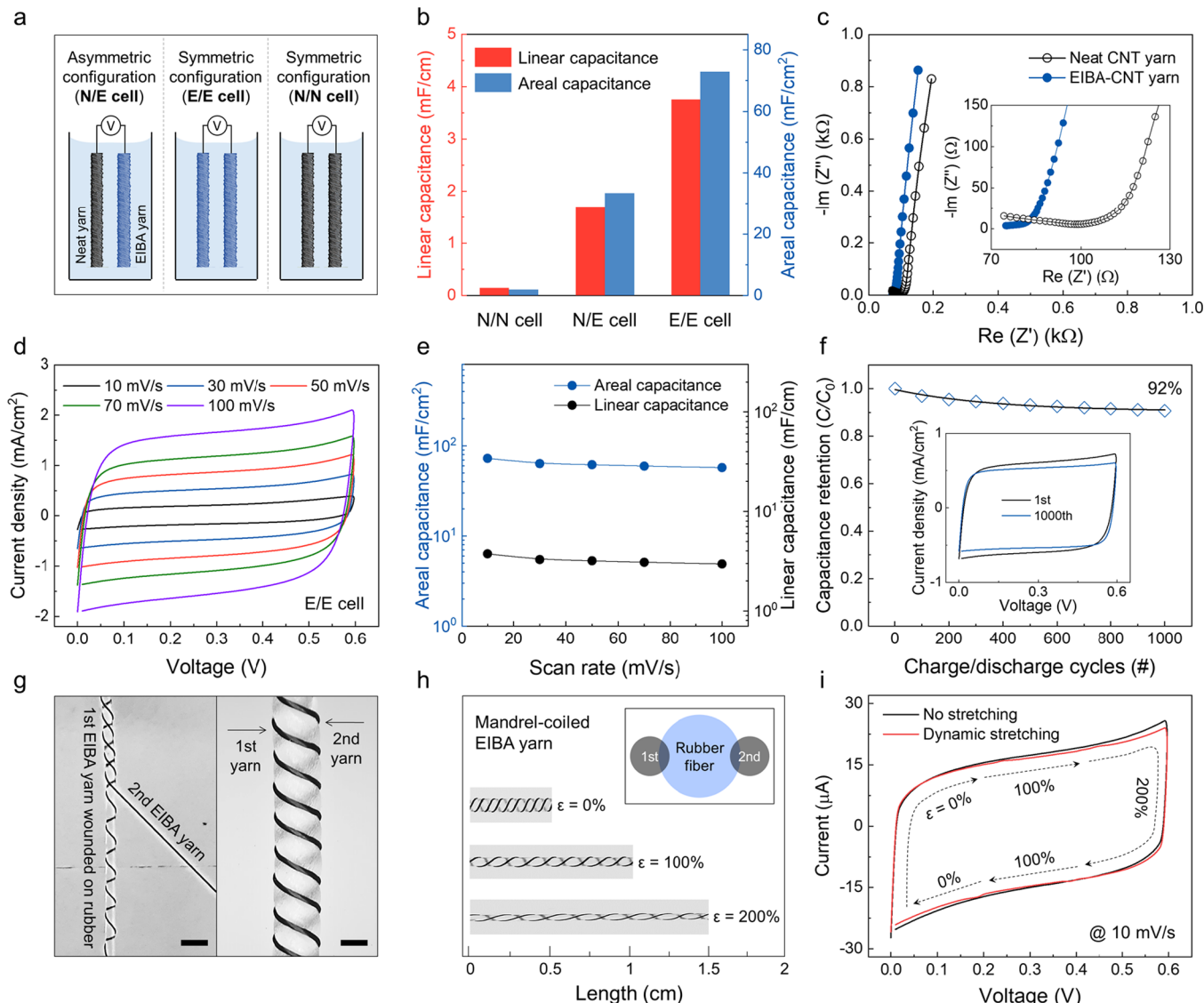


**Figure 4.** Electrochemical performance of the assembled EIBA-CNT yarn supercapacitors and mandrel coiling for stretching tolerance capability. (a) Illustration of the supercapacitor cell configurations for electrochemical performance characterization, where N and E indicate the neat and EIBA yarns, respectively. (b) Comparison of the linear and areal capacitance values of the N/N cell ( $0.21, 2.89\ \text{mF}/\text{cm}^2$ , respectively), N/E cell ( $1.71, 33.03\ \text{mF}/\text{cm}^2$ , respectively), and E/E cell ( $3.75, 72.81\ \text{mF}/\text{cm}^2$ , respectively). (c) Nyquist curves ( $0.2\ \text{Hz}$ – $100\ \text{kHz}$ ) of the neat CNT and EIBA-CNT yarns. Inset shows the high-frequency region. (d) CV curves of the E/E cell supercapacitor, measured from  $10$  to  $100\ \text{mV/s}$ . (e) Calculated single-electrode linear and areal capacitance values of the E/E cell supercapacitors at various scan rates. (f) Capacitance retention during repeated charge/discharge cycles. Inset shows a comparison between the first and 1000th CV curves at  $30\ \text{mV/s}$ , indicating  $92\%$  capacitance retention. (g) Photographs showing EIBA-CNT yarns helically wrapped onto a silicone rubber mandrel with a diameter of  $800\ \mu\text{m}$  (left image, scale bar: 2 mm) and the assembled mandrel-coiled EIBA-CNT yarn supercapacitor (right image, scale bar: 500  $\mu\text{m}$ ). (h) Images of the mandrel-coiled EIBA-CNT yarn supercapacitor before ( $\epsilon = 0\%$ ) and after strain application ( $\epsilon = 100\%$  and  $200\%$ ). (i) Measured CV curves (scan rate of  $10\ \text{mV/s}$ ) for the no stretching (black line) and dynamical stretching states (red line) (up to  $200\%$  strain).

torsional hydro-actuation for forward (water absorption) and reverse (water desorption) rotations during 10 cycles.

**Electrochemical Performance Characterization of the Assembled Supercapacitors with Stretching Tolerance by Mandrel Coiling.** Another remarkable effect of EIBA on the CNT yarns can be confirmed by exploring the electrochemical performances of the yarns before and after the EIBA process. Generally, the neat CNT yarns exhibit relatively low capacitance because of the limited ion accessibility derived from intrinsic hydrophobicity.<sup>49</sup> If the inert graphitic carbon framework of these CNT yarns is fully activated or functionalized, then a surge in the specific capacitance is

expected with the improved ion transfer between the yarn and the aqueous electrolyte. Particularly, oxygen-containing functional groups can provide reversible pseudocapacitance via successive redox mechanisms.<sup>50</sup> The resultant rapid and reversible ion adsorption/desorption considerably improves the specific capacitance compared to the electric double-layer capacitance (EDLC) of bare CNTs.<sup>49</sup>

Accordingly, the following three cell configurations were prepared to compare the electrochemical performances of the symmetrically or asymmetrically assembled two parallel CNT yarns: N/E cells, E/E cells, and N/N cells, where N and E represent the neat CNT and EIBA-CNT yarns, respectively

(Figure 4a). Cyclic voltammetry (CV) curves of the supercapacitors composed of each cell were plotted and analyzed at a scan rate of 10 mV/s (Figures S11 and 4b). The specific capacitances reported in this paper are normalized with respect to a single electrode. The symmetric N/N cell supercapacitor showed linear and areal capacitances (0.21 mF/cm and 2.89 mF/cm<sup>2</sup>, respectively), which were comparable to those obtained in previously reported studies (1.97–8.66 mF/cm<sup>2</sup>).<sup>51–53</sup> However, the asymmetric supercapacitor with the N/E cell configuration showed improved specific capacitances (1.71 mF/cm and 33.03 mF/cm<sup>2</sup>), which may be due to the higher electrochemical performance of the EIBA-CNT yarn (the electrochemical performance of the neat CNT yearns was relatively low). This is supported by the electrochemical impedance spectroscopy (EIS) results shown in Figure 4c. It was found that the impedance of the EIBA-CNT yarn was much smaller than that of the neat CNT yarn. Therefore, the symmetric supercapacitor consisting of E/E cells showed the largest CV curve (approximately 25 times that of the N/N cell supercapacitor) (Figure S11). The CV curves measured with scan rates from 10 to 100 mV/s for the E/E cell supercapacitor are presented in Figure 4d. The rectangular-like CV curve without any Faradaic redox peak is well consistent with the energy storage mechanism of an electrochemical double-layer capacitor, made from CNT, and the pseudocapacitance of the oxygen-containing groups. However, a highly distorted CV curve was obtained at a scan rate of 100 mV/s when excessive activation was performed (Figure S12), possibly owing to the drastic decrease in the electrical conductivity of the CNT yearns. Figure 4e shows the specific capacitance values of the E/E cell supercapacitors. High areal (72.81 mF/cm<sup>2</sup>) and linear capacitances (3.75 mF/cm) were achieved at the 10 mV/s scan rate. Compared with the performances of previously reported CNT-based supercapacitors containing pseudocapacitive guest materials (e.g., conducting polymers or transition-metal oxides) (Table S2),<sup>54–59</sup> this specific capacitance may still be unsatisfactory to facilitate the practical application of the CNT-yearn-based supercapacitors as power sources. However, it should be noted that these capacitances of the electrochemically-activated CNT yarn are remarkably higher than the intrinsic capacitance of the pure CNT yearns without any guest materials, indicating the possibility of constructing advanced supercapacitors. The E/E cell supercapacitor also showed a high electrochemical cycle capability with 92% capacitance retention even after 1000 charge/discharge cycles (Figure 4f).

Furthermore, one of the important features required for using yearns or fiber-based supercapacitors as power sources in wearable electronic devices is an excellent stretching tolerance. We adopted a mandrel-coil structure, fabricated by winding two symmetrical EIBA-CNT yearns around a mandrel elastomer (Figure 4g), to induce a large mechanical stretchability in the CNT yearn-based supercapacitors. A constant gap was maintained between the two yearns during the CNT yearn wrapping to prevent electrical shorting. Although the diameter of the used core mandrel was much larger (800 μm) than that of the CNT yearns, the stretchability of the latter could be significantly improved by changing either the gap distance between the yearns ( $d$ ) or the mandrel-coil bias angle ( $\beta$ ) or both (Figure 4h). Approximately no change in the resistance was observed while stretching by reversibly changing both  $d$  and  $\beta$  (increased  $d$  and decreased  $\beta$  when stretched), and a large stretchability of up to 200% was achieved (Figure S11). Therefore, we could achieve stable charge storage character-

istics of the mandrel-coiled EIBA-CNT yearn supercapacitor (Figure 4i).

## CONCLUSIONS

In summary, we developed an electrochemically inner-bundle-activated CNT yearn with a drastically enhanced performance, especially in terms of hydro-actuations and specific capacitances. Table S3 shows a detailed comparison of our results with those previously reported in the literature on electrochemical functionalization to clarify the novelty of the present work. The proposed EIBA process not only induces an electrolyte infiltration-driven volume expansion in the two-end tethered CNT yearn but also functionalizes the yearns with oxygen-containing groups. The resulting yearns experienced a dramatic change in wetting properties from hydrophobicity (CA of 120°) to hydrophilicity (CA of 38°). Benefiting from the electrolyte infiltration-induced inter-nanotube swelling and high water interactivity of the EIBA-treated CNT yearn, a large and fast hydro-actuation (~986 revolutions/m) was generated when the yearn was exposed to moisture or water. Moreover, the EIBA-introduced oxygen-containing groups produced a pseudocapacitive behavior in the EIBA-CNT yearns in an aqueous electrolyte system. The capacitance of the resulting yearn-based supercapacitor was significantly enhanced (25 times larger), more than that of the neat CNT yearn-based supercapacitor. These inner-bundle-activated CNT yearns can be used in various applications, including those in aqueous environments, as high-performance hydro-actuators, supercapacitors, and energy harvesters (from water).

## EXPERIMENTAL SECTION

**Preparation of the EIBA-CNT Yearns.** First, twenty 20-mm-wide and 50-mm-long CNT sheets, drawn from a MWNT forest (height: ~280 μm) (A-Tech System Co., Korea), were stacked to form a layered structure. Then, one end of this CNT stack was attached to the motor tip of the twisting machine (K6G3C, GGM), and the other end was supported by a load of ~3 g. After inserting a high twist of 1000 turns per meter into the stacks, uniform and straight CNT yearns (diameter of ~224 μm) were obtained. For a stable EIBA processing and electrochemical performance characterization, both the ends of the CNT yearns (length: 1 cm) were connected to Cu wires (diameter of 180 μm) and then chemically tethered using an epoxy glue (Devcon, USA). The EIBA process was performed using a three-electrode electrochemical system consisting of the CNT yearn (working electrode), Ag/AgCl (reference electrode), a Pt mesh (counter electrode), and 0.1 M Na<sub>2</sub>SO<sub>4</sub> (aqueous electrolyte). Next, a potentiostatic voltage (vs Ag/AgCl) was applied using an electrochemical analyzer (Vertex EIS, Ivium).

**Characterizations.** The optical images of the CNT yearns were obtained using a microscope (D750, Nikon), and the detailed surface morphology of the yearn was identified from the SEM (S-4600, Hitachi, Japan) images. A slow-motion video was captured by a high-speed camera (RX10 IV, SONY). The chemical composition and features of the CNT yearns were determined by XPS measurements performed using ESCALAB 250XI (Thermo Scientific). The mechanical properties were measured by a universal testing machine with a strain rate of 1 mm per minute.

**Measurement of Hydration-Driven Actuation.** The EIBA-CNT yearn was vertically hung on an actuation test setup by fixing one end using a carbon tape and epoxy glue. A Cu rod (weight: 10 mg) with a length of 15 mm and diameter of 255 μm was attached at the bottom end of the CNT yearn as a paddle for the torsional actuation measurement. The RH during the testing was adjusted by supplying moisture from a humidifier or by flowing dry N<sub>2</sub> gas in a homemade container equipped with a hygrometer. All the generated torsional

actuation was recorded in slow motion (480 frames/s), and the movie frames were analyzed.

**Electrical Measurements.** A cylindrical neodymium magnet (20 mg) was attached at the bottom end of the EIBA-CNT yarn. Three coil-shaped inductors, each with a diameter of 10 mm and length of 24 mm, were extracted from a commercially available watch. The magnet was placed at the center of the triple-solenoid coil, and a constant distance was maintained during the torsional actuation. The voltage induced from the coil inductors was analyzed using an oscilloscope (DSOX2024A, KEYSIGHT).

**Measurement and Calculation of Electrochemical Performance.** An electrochemical analyzer was used to perform all the electrochemical tests, including CV and EIS. The capacitance of a single electrode in the CNT yarn supercapacitor ( $C$ ) was calculated from CV curves using eq 1:

$$C = I/(dV/dt) \quad (1)$$

where  $I$  denotes the average discharge current, and  $dV/dt$  represents the scan rate. The specific capacitance ( $C_{sp}$ ) was calculated using eq 2:

$$C_{sp} = 2C/\text{Unit} \quad (2)$$

where Unit is the total length or total surface area of the CNT yarn, assumed to be cylindrical for linear and areal capacitances.

**Mandrel Coiling of the EIBA-CNT Yarns.** Mandrel-coiled yarns were constructed by winding the CNT yarns around a 200% pre-stretched silicone rubber mandrel with a diameter of 800  $\mu\text{m}$ . The CNT yarns were tightly packed on the mandrel during the stretching and releasing processes.

**Computational Details.** The Vienna ab-initio simulation package with van der Waals correction was employed for the DFT calculations. The project-augmented wave potential was utilized with the generalized gradient approximation within the Perdew–Burke–Ernzerhof framework. A  $4 \times 4$  bilayer graphene sheet modeled with 64 carbon atoms was constructed with a vacuum spacing of 15  $\text{\AA}$ . A  $\Gamma$ -centered  $k$ -point mesh of  $4 \times 4 \times 1$  was used to sample the two-dimensional Brillouin zone. The atomic positions were optimized according to the atomic forces under the criterion that the calculated force on each atom should be smaller than 0.01 eV/ $\text{\AA}$ . The criterion for energy convergence was  $10^{-5}$  eV/cell. The interlayer distance of the bilayer graphene with various oxygen functional groups was calculated using eq 3.

$$L = H_{\text{top layer}} - H_{\text{bottom layer}} \quad (3)$$

where  $L$  is the interlayer distance of bilayer graphene, and  $H$  is the average  $z$ -coordination of the carbon atoms in the top and bottom layers. The water-driven expansion length of CNT interlayers was calculated using eq 4.

$$\Delta L = L_{\text{C+H}_2\text{O}} - L_C \quad (4)$$

where  $\Delta L$  is the water-driven expansion length of the CNT interlayers, and  $L_{\text{C+H}_2\text{O}}$  and  $L_C$  are the interlayer distances of the wet and dry bilayer graphene, respectively.

## ASSOCIATED CONTENT

### Supporting Information

The Supporting Information is available free of charge at <https://pubs.acs.org/doi/10.1021/acsami.2c20666>.

Electrochemical activation condition; input power competitive table with previous reports; SEM images of neat and EIBA-CNT yarns; Raman and XPS spectra of neat and EIBA-CNT yarns; application of EIBA-CNT yarns; bias angle changes of EIBA-CNT yarns with different twist insertion; torsional actuation performances of EIBA-CNT yarns with different twist insertion; CV curves of different cell configurations; CV curve of excessive EIBA-CNT yarns; and characterization of Mandrel-coiled EIBA-CNT yarn supercapacitors (PDF)

Nano-gaps in the aligned CNTs within the yarn undergoing drastic expansion with the increased internal pressure (MP4)

## AUTHOR INFORMATION

### Corresponding Authors

Seon Jeong Kim – Center for Self-Powered Actuation, Department of Electronic Engineering, Hanyang University, Seoul 04763, South Korea;  [orcid.org/0000-0002-2867-6737](https://orcid.org/0000-0002-2867-6737); Email: [sjk@hanyang.ac.kr](mailto:sjk@hanyang.ac.kr)

Changsoon Choi – Department of Energy and Materials Engineering, Dongguk University, Seoul 04620, Republic of Korea;  [orcid.org/0000-0003-4456-4548](https://orcid.org/0000-0003-4456-4548); Email: [cschoi84@dongguk.edu](mailto:cschoi84@dongguk.edu)

### Authors

Wonkyeong Son – Department of Energy and Materials Engineering, Dongguk University, Seoul 04620, Republic of Korea; Department of Energy Science, Sungkyunkwan University, Suwon 16419, Republic of Korea

Jae Myeong Lee – Department of Energy and Materials Engineering, Dongguk University, Seoul 04620, Republic of Korea; Center for Self-Powered Actuation, Department of Electronic Engineering, Hanyang University, Seoul 04763, South Korea

Sungwoo Chun – Department of Electronics and Information Engineering, Korea University, Sejong 30019, Republic of Korea

Seongjun Yu – Department of Energy and Materials Engineering, Dongguk University, Seoul 04620, Republic of Korea

Jun Ho Noh – Department of Energy and Materials Engineering and Department of Advanced Battery Convergence Engineering, Dongguk University, Seoul 04620, Republic of Korea

Hyeon Woo Kim – Center of Materials Digitalization, Korea Institute of Ceramic Engineering and Technology (KICET), Jinju-si 52851, Republic of Korea; Division of Materials Science and Engineering, Hanyang University, Seoul 04763, Republic of Korea

Sung Beom Cho – Center of Materials Digitalization, Korea Institute of Ceramic Engineering and Technology (KICET), Jinju-si 52851, Republic of Korea; Department of Materials Science and Engineering, Ajou University, Suwon 16499, Republic of Korea

Complete contact information is available at: <https://pubs.acs.org/10.1021/acsami.2c20666>

### Author Contributions

W.S. and J.M.L. contributed equally to this work.

### Author Contributions

W.S., J.M.L., S.J.K., and C.C. conceptualized the idea and designed the experiments. J.H.N., S.C., and S.Y. performed the experiments and analyzed the experimental results. H.W.K. and S.B.C. performed the simulation works. All authors contributed to writing the manuscript.

### Notes

The authors declare no competing financial interest.

## ACKNOWLEDGMENTS

This work was supported by the Korea Institute of Energy Technology Evaluation and Planning (KETEP) and the

Ministry of Trade, Industry & Energy (MOTIE) of the Republic of Korea (No. 20224000000020) and the Creative Research Initiative Center for Self-Powered Actuation in the National Research Foundation of Korea.

## ■ REFERENCES

- (1) Zhang, M.; Atkinson, K. R.; Baughman, R. H. Multifunctional Carbon Nanotube Yarns by Downsizing an Ancient Technology. *Science* **2004**, *306*, 1358–1361.
- (2) Foroughi, J.; Spinks, G. M.; Wallace, G. G.; Oh, J.; Kozlov, M. E.; Fang, S.; Mirfakhrai, T.; Madden, J. D.; Shin, M. K.; Kim, S. J.; Baughman, R. H. Torsional Carbon Nanotube Artificial Muscles. *Science* **2011**, *334*, 494–497.
- (3) Choi, C.; Lee, J. A.; Choi, A. Y.; Kim, Y. T.; Lepró, X.; Lima, M. D.; Baughman, R. H.; Kim, S. J. Flexible Supercapacitor Made of Carbon Nanotube Yarn with Internal Pores. *Adv. Mater.* **2014**, *26*, 2059–2065.
- (4) Wepasnick, K. A.; Smith, B. A.; Schrote, K. E.; Wilson, H. K.; Diegelmann, S. R.; Fairbrother, D. H. Surface and Structural Characterization of Multi-Walled Carbon Nanotubes Following Different Oxidative Treatments. *Carbon* **2011**, *49*, 24–36.
- (5) Saka, C. Overview on the Surface Functionalization Mechanism and Determination of Surface Functional Groups of Plasma Treated Carbon Nanotubes. *Crit. Rev. Anal. Chem.* **2018**, *48*, 1–14.
- (6) Ham, S. W.; Hong, H. P.; Kim, J. H.; Min, S. J.; Min, N. K. Effect of Oxygen Plasma Treatment on Carbon Nanotube-Based Sensors. *J. Nanosci. Nanotechnol.* **2014**, *14*, 8476–8481.
- (7) Lei, C.; Lyu, S.; Si, J.; Yang, B.; Li, Z.; Lei, L.; Wen, Z.; Wu, G.; Hou, Y. Nanostructured Carbon Based Heterogeneous Electrocatalysts for Oxygen Evolution Reaction in Alkaline Media. *ChemCatChem* **2019**, *11*, 5855–5874.
- (8) Yu, H.; Cheng, D.; Williams, T. S.; Severino, J.; De Rosa, I. M.; Carlson, L.; Hicks, R. F. Rapid Oxidative Activation of Carbon Nanotube Yarn and Sheet by a Radio Frequency, Atmospheric Pressure Helium and Oxygen Plasma. *Carbon* **2013**, *57*, 11–21.
- (9) He, S.; Chen, P.; Qiu, L.; Wang, B.; Sun, X.; Xu, Y.; Peng, H. A Mechanically Actuating Carbon-Nanotube Fiber in Response to Water and Moisture. *Angew. Chem., Int. Ed. Engl.* **2015**, *54*, 14880–14884.
- (10) He, S.; Hu, Y.; Wan, J.; Gao, Q.; Wang, Y.; Xie, S.; Qiu, L.; Wang, C.; Zheng, G.; Wang, B.; Peng, H. Biocompatible Carbon Nanotube Fibers for Implantable Supercapacitors. *Carbon* **2017**, *122*, 162–167.
- (11) Shao, Y.; Xu, F.; Marriam, I.; Liu, W.; Gao, Z.; Qiu, Y. Quasi-Static and Dynamic Interfacial Evaluations of Plasma Functionalized Carbon Nanotube Fiber. *Appl. Surf. Sci.* **2019**, *465*, 795–801.
- (12) Adusei, P. K.; Gbordzoe, S.; Kanakaraj, S. N.; Hsieh, Y. Y.; Alvarez, N. T.; Fang, Y.; Johnson, K.; McConnell, C.; Shanov, V. Fabrication and Study of Supercapacitor Electrodes Based on Oxygen Plasma Functionalized Carbon Nanotube Fibers. *J. Energy Chem.* **2020**, *40*, 120–131.
- (13) Lavagna, L.; Nisticò, R.; Musso, S.; Pavese, M. Functionalization as a Way to Enhance Dispersion of Carbon Nanotubes in Matrices: A Review. *Mater. Today Chem.* **2021**, *20*, No. 100477.
- (14) Egetenmeyer, A.; Radev, I.; Durneata, D.; Baumgärtner, M.; Peinecke, V.; Natter, H.; Hempelmann, R. Pulse Electrodeposited Cathode Catalyst Layers for PEM Fuel Cells. *Int. J. Hydrogen Energy* **2017**, *42*, 13649–13660.
- (15) Jung, U.; Kim, H. S.; Jeong, H. S.; Suhr, J.; Kim, T. H.; Lee, H. Plasma Functionalization of Carbon Nanotubes and Radical Penetration Mechanism. *Plasma Processes Polym.* **2022**, *19*, No. 2200010.
- (16) Jiang, B.; Zheng, J.; Qiu, S.; Wu, M.; Zhang, Q.; Yan, Z.; Xue, Q. Review on Electrical Discharge Plasma Technology for Wastewater Remediation. *Chem. Eng. J.* **2014**, *236*, 348–368.
- (17) Lu, X.; Yim, W. L.; Suryanto, B. H. R.; Zhao, C. Electrocatalytic Oxygen Evolution at Surface-Oxidized Multiwall Carbon Nanotubes. *J. Am. Chem. Soc.* **2015**, *137*, 2901–2907.
- (18) Liang, Y.; Luo, X.; Weng, W.; Hu, Z.; Zhang, Y.; Xu, W.; Bi, Z.; Zhu, M. Activated Carbon Nanotube Fiber Fabric as a High-Performance Flexible Electrode for Solid-State Supercapacitors. *ACS Appl. Mater. Interfaces* **2021**, *13*, 28433–28441.
- (19) Lebron-Colon, M.; Meador, M. A.; Lukco, D.; Sola, F.; Santos-Perez, J.; McCorkle, L. S. Surface Oxidation Study of Single Wall Carbon Nanotubes. *Nanotechnology* **2011**, *22*, No. 455707.
- (20) Aumanen, J.; Johansson, A.; Koivistoinen, J.; Myllyperkiö, P.; Pettersson, M. Patterning and Tuning of Electrical and Optical Properties of Graphene by Laser Induced Two-Photon Oxidation. *Nanoscale* **2015**, *7*, 2851.
- (21) Wang, K.; Li, M.; Liu, Y. N.; Gu, Y.; Li, Q.; Zhang, Z. Effect of Acidification Conditions on the Properties of Carbon Nanotube Fibers. *Appl. Surf. Sci.* **2014**, *292*, 469–474.
- (22) Ye, J. S.; Liu, X.; Cui, H. F.; Zhang, W. D.; Sheu, F. S.; Lim, T. M. Electrochemical Oxidation of Multi-Walled Carbon Nanotubes and Its Application to Electrochemical Double Layer Capacitors. *Electrochim. Commun.* **2005**, *7*, 249–255.
- (23) Liu, C. M.; Cao, H. B.; Li, Y. P.; Xu, H. B.; Zhang, Y. The Effect of Electrolytic Oxidation on the Electrochemical Properties of Multi-Walled Carbon Nanotubes. *Carbon* **2006**, *44*, 2919–2924.
- (24) Tang, H.; Chen, J.; Nie, L.; Yao, S.; Kuang, Y. Electrochemical Oxidation of Glutathione at Well-Aligned Carbon Nanotube Array Electrode. *Electrochim. Acta* **2006**, *51*, 3046–3051.
- (25) Balasubramanian, K.; Burghard, M. Electrochemically Functionalized Carbon Nanotubes for Device Applications. *J. Mater. Chem.* **2008**, *18*, 3071–3083.
- (26) Gao, G.; Pan, M.; Vecitis, C. D. Effect of the Oxidation Approach on Carbon Nanotube Surface Functional Groups and Electrooxidative Filtration Performance. *J. Mater. Chem. A* **2015**, *3*, 7575.
- (27) Moraitis, G.; Špitálský, Z.; Ravani, F.; Siokou, A.; Galiotis, C. Electrochemical Oxidation of Multi-Wall Carbon Nanotubes. *Carbon* **2011**, *49*, 2702–2708.
- (28) Senokos, E.; Rana, M.; Santos, C.; Marcilla, R.; Vilatela, J. J. Controlled Electrochemical Functionalization of CNT Fibers: Structure-Chemistry Relations and Application in Current Collector-Free All-Solid Supercapacitors. *Carbon* **2019**, *142*, 599–609.
- (29) Kim, J. W.; Sauti, G.; Siochi, E. J.; Smith, J. G.; Wincheski, R. A.; Cano, R. J.; Connell, J. W.; Wise, K. E. Toward High Performance Thermoset/Carbon Nanotube Sheet Nanocomposites Via Resistive Heating Assisted Infiltration and Cure. *ACS Appl. Mater. Interfaces* **2014**, *6*, 18832–18843.
- (30) Ma, W.; Liu, L.; Yang, R.; Zhang, T.; Zhang, Z.; Song, L.; Ren, Y.; Shen, J.; Niu, Z.; Zhou, W.; Xie, S. Monitoring a Micromechanical Process in Macroscale Carbon Nanotube Films and Fibers. *Adv. Mater.* **2009**, *21*, 603–608.
- (31) Qiu, J.; Terrones, J.; Vilatela, J. J.; Vickers, M. E.; Elliott, J. A.; Windle, A. H. Liquid Infiltration into Carbon Nanotube Fibers: Effect on Structure and Electrical Properties. *ACS Nano* **2013**, *7*, 8412–8422.
- (32) Chen, P.; Xu, Y.; He, S.; Sun, X.; Pan, S.; Deng, J.; Chen, D.; Peng, H. Hierarchically Arranged Helical Fibre Actuators Driven by Solvents and Vapours. *Nat. Nanotechnol.* **2015**, *10*, 1077–1083.
- (33) Wang, Y.; Qiao, J.; Wu, K.; Yang, W.; Ren, M.; Dong, L.; Zhou, Y.; Wu, Y.; Wang, X.; Yong, Z.; Di, J.; Li, Q. High-Twist-Pervaded Electrochemical Yarn Muscles with Ultralarge and Fast Contractile Actuations. *Mater. Horiz.* **2020**, *7*, 3043–3050.
- (34) Mu, J.; Jung de Andrade, M.; Fang, S.; Wang, X.; Gao, E.; Li, N.; Kim, S. H.; Wang, H.; Hou, C.; Zhang, Q.; Zhu, M.; Qian, D.; Lu, H.; Kongahage, D.; Talebian, S.; Foroughi, J.; Spinks, G.; Kim, H.; Ware, T. H.; Sim, H. J.; Lee, D. Y.; Jang, Y.; Kim, S. J.; Baughman, R. H. Sheath-Run Artificial Muscles. *Science* **2019**, *365*, 150–155.
- (35) Lima, M. D.; Li, N.; Jung de Andrade, M.; Fang, S.; Oh, J.; Spinks, G. M.; Kozlov, M. E.; Haines, C. S.; Suh, D.; Foroughi, J.; Kim, S. J.; Chen, Y.; Ware, T.; Shin, M. K.; Machado, L. D.; Fonseca, A. F.; Madden, J. D.; Voit, W. E.; Galvao, D. S.; Baughman, R. H. Chemically, and Photonically Powered Torsional and Tensile

- Actuation of Hybrid Carbon Nanotube Yarn Muscles. *Science* **2012**, *338*, 928–932.
- (36) Gu, X.; Fan, Q.; Yang, F.; Cai, L.; Zhang, N.; Zhou, W.; Zhou, W.; Xie, S. Hydro-Actuation of Hybrid Carbon Nanotube Yarn Muscles. *Nanoscale* **2016**, *8*, 17881–17886.
- (37) Wang, W.; Xiang, C.; Liu, Q.; Li, M.; Zhong, W.; Yan, K.; Wang, D. Natural Alginate Fiber-Based Actuator Driven by Water or Moisture for Energy Harvesting and Smart Controller Applications. *J. Mater. Chem. A* **2018**, *6*, 22599–22608.
- (38) Marega, R.; Accorsi, G.; Meneghetti, M.; Parisini, A.; Prato, M.; Bonifazi, D. Cap Removal and Shortening of Double-Walled and Very-Thin Multi-Walled Carbon Nanotubes under Mild Oxidative Conditions. *Carbon* **2009**, *47*, 675–682.
- (39) Lai, C. C.; Lo, C. T. Plasma Oxidation of Electrospun Carbon Nanofibers as Supercapacitor Electrodes. *RSC Adv.* **2015**, *5*, 38868–38872.
- (40) Ghanashyam, G.; Jeong, H. K. Synthesis of Nitrogen-Doped Plasma Treated Carbon Nanofiber as an Efficient Electrode for Symmetric Supercapacitor. *J. Energy Storage* **2021**, *33*, No. 102150.
- (41) He, S.; Zhang, Y.; Qiu, L.; Zhang, L.; Xie, Y.; Pan, J.; Chen, P.; Wang, B.; Xu, X.; Hu, Y.; Dinh, C. T.; De Luna, P.; Banis, M. N.; Wang, Z.; Sham, T. K.; Gong, X.; Zhang, B.; Peng, H.; Sargent, E. H. Chemical-to-Electricity Carbon: Water Device. *Adv. Mater.* **2018**, *30*, No. e1707635.
- (42) Beese, A. M.; Sarkar, S.; Nair, A.; Naraghi, M.; An, Z.; Moravsky, A.; Loutfy, R. O.; Buehler, M. J.; Nguyen, S. T.; Espinosa, H. D. Bio-Inspired Carbon Nanotube-Polymer Composite Yarns with Hydrogen Bond Mediated Lateral Interactions. *ACS Nano* **2013**, *7*, 3434–3446.
- (43) Shin, M. K.; Lee, B.; Kim, S. H.; Lee, J. A.; Spinks, G. M.; Gambhir, S.; Wallace, G. G.; Kozlov, M. E.; Baughman, R. H.; Kim, S. J. Synergistic Toughening of Composite Fibres by Self-Alignment of Reduced Graphene Oxide and Carbon Nanotubes. *Nat. Commun.* **2012**, *3*, 650.
- (44) Trivedi, D.; Rahn, C. D.; Kier, W. M.; Walker, I. D. Soft Robotics: Biological Inspiration, State of the Art, and Future Research. *Appl. Bionics Biomech.* **2008**, *5*, 99–117.
- (45) Li, Y.; Leng, X.; Sun, J.; Zhou, X.; Wu, W.; Chen, H.; Liu, Z. Moisture-Sensitive Torsional Cotton Artificial Muscle and Textile. *Chin. Phys. B* **2020**, *29*, No. 048103.
- (46) Xu, P.; Gu, T.; Cao, Z.; Wei, B.; Yu, J.; Li, F.; Byun, J. H.; Lu, W.; Li, Q.; Chou, T. W. Carbon Nanotube Fiber Based Stretchable Wire-Shaped Supercapacitors. *Adv. Energy Mater.* **2014**, *4*, No. 1300759.
- (47) Cheng, H.; Hu, Y.; Zhao, F.; Dong, Z.; Wang, Y.; Chen, N.; Zhang, Z.; Qu, L. Moisture-Activated Torsional Graphene-Fiber Motor. *Adv. Mater.* **2014**, *26*, 2909–2913.
- (48) Chen, H.; Ye, S.; Tao, Q.; Chen, Z.; Tu, Y.; Yang, X. Hygroresponsive Torsional Yarns and Actuators Based on Cascade Amplification of the Deformation. *Macromol. Mater. Eng.* **2021**, *306*, No. 2000822.
- (49) Frackowiak, E.; Béguin, F. Carbon materials for the electrochemical storage of energy in capacitors. *Carbon* **2001**, *39*, 937–950.
- (50) Xiao, X.; Li, T.; Peng, Z.; Jin, H.; Zhong, Q.; Hu, Q.; Yao, B.; Luo, Q.; Zhang, C.; Gong, L.; Chen, J.; Gogotsi, Y.; Zhou, J. Freestanding Functionalized Carbon Nanotube-Based Electrode for Solid-State Asymmetric Supercapacitors. *Nano Energy* **2014**, *6*, 1–9.
- (51) Chen, X.; Qiu, L.; Ren, J.; Guan, G.; Lin, H.; Zhang, Z.; Chen, P.; Wang, Y.; Peng, H. Novel Electric Double-Layer Capacitor with a Coaxial Fiber Structure. *Adv. Mater.* **2013**, *25*, 6436–6441.
- (52) Ren, J.; Li, L.; Chen, C.; Chen, X.; Cai, Z.; Qiu, L.; Wang, Y.; Zhu, X.; Peng, H. Twisting Carbon Nanotube Fibers for Both Wire-Shaped Micro-Supercapacitor and Micro-Battery. *Adv. Mater.* **2013**, *25*, 1224.
- (53) Ren, J.; Bai, W.; Guan, G.; Zhang, Y.; Peng, H. Flexible and Weaveable Capacitor Wire Based on a Carbon Nanocomposite Fiber. *Adv. Mater.* **2013**, *25*, 5965–5970.
- (54) Su, F.; Miao, M.; Niu, H.; Wei, Z. Gamma-Irradiated Carbon Nanotube Yarn As Substrate for High-Performance Fiber Supercapacitors. *ACS Appl. Mater. Interfaces* **2014**, *6*, 2553–2560.
- (55) Lyu, W.; Zhang, W.; Liu, H.; Liu, Y.; Zuo, H.; Yan, C.; Faul, C. F. J.; Thomas, A.; Zhu, M.; Liao, Y. Conjugated Microporous Polymer Network Grafted Carbon Nanotube Fibers with Tunable Redox Activity for Efficient Flexible Wearable Energy Storage. *Chem. Mater.* **2020**, *32*, 8276–8285.
- (56) Choi, C.; Kim, K. M.; Kim, K. J.; Lepró, X.; Spinks, G. M.; Baughman, R. H.; Kim, S. J. Improvement of System Capacitance Via Weavable Superelastic Biscrolled Yarn Supercapacitors. *Nat. Commun.* **2016**, *7*, 13811.
- (57) Kim, J. H.; Choi, C.; Lee, J. M.; de Andrade, M. J.; Baughman, R. H.; Kim, S. J. Ag/MnO<sub>2</sub> Composite Sheath-Core Structured Yarn Supercapacitors. *Sci. Rep.* **2018**, *8*, 13309.
- (58) Su, F.; Lv, X.; Miao, M. High-Performance Two-Ply Yarn Supercapacitors Based on Carbon Nanotube Yarns Dotted with Co<sub>3</sub>O<sub>4</sub> and NiO Nanoparticles. *Small* **2015**, *11*, 854–861.
- (59) Pan, Z.; Yang, J.; Zhang, Q.; Liu, M.; Hu, Y.; Kou, Z.; Liu, N.; Yang, X.; Ding, X.; Chen, H.; Li, J.; Zhang, K.; Qiu, Y.; Li, Q.; Wang, J.; Zhang, Y. All-Solid-State Fiber Supercapacitors with Ultrahigh Volumetric Energy Density and Outstanding Flexibility. *Adv. Energy Mater.* **2019**, *9*, No. 1802753.

**CAS INSIGHTS™****EXPLORE THE INNOVATIONS SHAPING TOMORROW**

Discover the latest scientific research and trends with CAS Insights. Subscribe for email updates on new articles, reports, and webinars at the intersection of science and innovation.

Subscribe today

